universe

MDPI

Article

Short-Term Consequences of Asteroid Impacts into the Ocean: A Portuguese Case Study

Renato H. Morais [1], Luís F. F. M. Santos [1,2], André R. R. Silva [1] and Rui Melicio [3,4,*]

[1] LAETA-AEROG, Universidade da Beira Interior, 6200-358 Covilhã, Portugal; renatohenriques2@hotmail.com (R.H.M.); luis.santos@iseclisboa.pt (L.F.F.M.S.); andre@ubi.pt (A.R.R.S.)
[2] ISEC Lisboa, 1750-142 Lisbon, Portugal
[3] LAETA-IDMEC, Instituto Superior Técnico, Universidade de Lisboa, 1049-001 Lisbon, Portugal
[4] ICT, Escola de Ciências e Tecnologia, Universidade de Évora, 7002-554 Évora, Portugal
* Correspondence: ruimelicio@gmail.com

Abstract: Asteroid impacts are a proven global threat, meaning that any location on Earth might be a subject to their consequences. Such collisions are not likely in any person's lifetime, but their aftermath could be catastrophic. As Earth's surface is mostly water, a water impact is more probable than a ground impact, and tsunami waves could pose a significant threat. This study expands the knowledge about asteroid impacts in the ocean and their regional environmental consequences. Three asteroids were assumed to impact the Earth: (1) the Apophis asteroid, a 370 m wide asteroid, (2) a 204 m in diameter asteroid representative of the average impactor on the near-Earth objects, and (3) a 5 km in diameter asteroid. We evaluated the consequences of all impacts for a specific case study, where the chosen impact location was the midpoint between Portugal's mainland, Azores, and Madeira Islands. The cratering process, generated seismic shaking, overpressure, ejected material, induced thermal radiation, and tsunami waves were assessed, along with the global effects. The overpressure mainly causes structural damage. The thermal radiation can be devastating but has a short reach. The tsunami is undoubtedly the most far-reaching and threatening effect of an asteroid impact in the ocean.

Keywords: Apophis; medium asteroid; 5 km impactor; impact effects; vulnerabilities; casualties

check for updates

Citation: Morais, R.H.; Santos, L.F.F.M.; Silva, A.R.R.; Melicio, R. Short-Term Consequences of Asteroid Impacts into the Ocean: A Portuguese Case Study. *Universe* **2022**, *8*, 279. https://doi.org/10.3390/universe8050279

Academic Editors: Elizabeth A. Silber, Maria Gritsevich and Josep Maria Trigo-Rodríguez

Received: 5 April 2022
Accepted: 3 May 2022
Published: 10 May 2022

Publisher's Note: MDPI stays neutral with regard to jurisdictional claims in published maps and institutional affiliations.

Copyright: © 2022 by the authors. Licensee MDPI, Basel, Switzerland. This article is an open access article distributed under the terms and conditions of the Creative Commons Attribution (CC BY) license (https://creativecommons.org/licenses/by/4.0/).

1. Introduction

Earth has been the target of asteroid impacts since its creation. Collisions with hazardous asteroids are not frequent, but studying them is still relevant, as they can pose a threat to populations.

The Apophis asteroid was first discovered in 2004 and has an estimated 370 m diameter [1,2]. It is one of the best-known asteroids because the initial observation predicted a high probability of impact in 2029, reaching an unprecedented value of four on the Torino scale [3]. This possibility of impact in 2029 was disregarded with updated observations [4]. However, a future impact in 2036 remained a possibility [5]. Newer observations denied this possibility [6], and the value of 0 was reassigned to Apophis. Based on its orbit and spectral type, Apophis is an Aten and Sq-type asteroid [7]. Aten asteroids have Earth-crossing orbits with a semi-major axis of less than 1.0 AU (astronomical unit) and an aphelion greater than 0.983 AU. Sq asteroids have siliceous mineralogical compositions with the presence of metal. According to observations made, Apophis resembles an LL ordinary chondrite, i.e., a group of stony meteorites, which allowed the estimation of its bulk density as 3.2 g·cm^{-3} [8]. A previous study already modelled the impact of Apophis into the ocean and studied its consequences in detail [9].

NASA keeps track of all near-Earth objects (NEOs), asteroids, and comets with perihelion distances of less than 1.3 AU [10]. All these objects were used in assessing the average asteroid diameter that could threaten Earth and its populations. Between 10 March 2020

and 26 November 2200, there are several thousand celestial objects with a close approach nominal distance of less than 0.05 AU. The average impact velocity and diameter of these objects are 10.84 km·s^{-1} and 204 m, respectively. A density value of 3100 kg·m^{-3} was assigned in [11] as a representative value for an asteroid population.

An asteroid of 5 km in diameter was also predicted to impact the Earth. Collisions of this magnitude only happen approximately once every twenty million years [12]. The asteroid's density was 2500 kg·m^{-3}, considering the average value for sedimentary rock [13]. The impact velocity was 15 km·s^{-1} because this is the threshold for vaporisation to occur that induces thermal radiation, as stated in [14].

Several authors have studied and modelled the impacts of external bodies on Earth. Algorithms to determine the principal impact effects that might affect people, infrastructures, and landscapes in the surroundings of an impact event were already published [14]. These algorithms estimate the asteroid's atmospheric entry, the thermal radiation emitted, the seismic shock intensity, the impact crater dimensions, the ejecta deposits, and the severity of air blast from airbursts or ground impacts.

The virtual impacts of 315 asteroids included on NASA's NEO risk list were assessed in [15]. This assessment included the impact location probability distribution. Later, the impact corridors for 261 observed asteroids that could impact the Earth before 2100 were reassessed [16]. Afterwards, the corridors were projected onto the Earth's map, considering the impact probability distributions. The cumulative impact probability distribution was paired with Earth's population to produce a risk map to recognise which nations are more prone to danger by an asteroid impact [17–19].

A tool to assess the impact risks of hazardous asteroids was developed and published [13]. The software expresses the risk in terms of expected casualties and allows comparisons with other natural phenomena. The authors also derived and presented vulnerability models that associate the severity of impact effects with the human population.

The probability of a water impact on Earth is higher than that of a land impact because the surface of the Earth is 71% water. Thus, most of the past asteroid impacts on Earth must have occurred in marine environments. Water impacts generate two distinct tsunami waves, rim waves and collapse waves, which have little in common with the traditional earthquake-induced tsunami waves. In addition, a water depth of 6–8 times the diameter of a stony asteroid is enough to completely suppress the cratering process in the benthic layer [20].

The main contributions are: (i) development of an analytical method, tested numerically by software, to assess the consequences of an impact event in the ocean; (ii) comparison of the impact consequences of three different sized asteroids; (iii) Portuguese vulnerability case study of independent municipalities.

2. Modelling

We followed a symbolic-numerical calculation to obtain the data for each point of interest while considering several premises to get more direct results. The impact was assumed to happen between mainland Portugal, Madeira, and the Azores, so no additional orbital mechanics calculations were required. The population was not warned about the threat, since it would be impossible to obtain the population vulnerability otherwise. Only direct effects were taken into account, so atmospheric, terrain, and wave reflections were not considered.

The haversine formula was used to obtain the midpoint between Portugal's mainland, Azores, and Madeira Islands, which determines the great-circle distance between two points on a sphere's surface. The distance from the impact site to the point of interest was found by (1):

$$D = R_E \arccos[\sin\phi_i \sin\phi_k + \cos\phi_i \cos\phi_k \cos(|\lambda_i - \lambda_k|)] \quad (1)$$

where D is the distance to the impact site, R_E is the radius of the Earth, ϕ and λ are the latitude and longitude, and the coefficients i and k represent the impact location and the point of interest, respectively.

The asteroid's destructive capabilities are directly related to the impact energy, which is a function of the impact angle and speed. In this analysis, there were two moments of interest. The first was the impact on the water surface, at sea level; the second was the impact with the ocean floor. In [14], we found a simple relation that allowed the estimation of the effect of a water layer on the asteroid's velocity. The equation computes the impactor's velocity at the sea floor, $v_{i_{seafloor}}$, as a function of the impactor's velocity at the surface, $v_{i_{surface}}$, as:

$$v_{i_{seafloor}} = v_{i_{surface}} e^{\frac{3\rho_w C_D h_{sea}}{2\rho_i L \sin\theta}} \tag{2}$$

where ρ_w and ρ_i are the water and impactor densities, h_{sea} is the depth of the ocean floor, L is the diameter of the impactor, θ is the impact angle, and C_D is the drag coefficient for a rigid sphere in the supersonic regime, which was set to 0.887 by the authors.

Using both impact velocities, $v_{i_{seafloor}}$ and $v_{i_{surface}}$, the impact energy at the surface $E_{surface}$, and consequently at the sea floor $E_{seafloor}$, were obtained. The air blast and thermal radiation models assumed that the impact energy responsible for these effects was released at the surface ($E = E_{surface}$). On the other hand, the seismic shaking and ejecta deposition originated from solid target impacts. Thus, the impact energy was assumed to be the kinetic energy from the impactor reaching the ocean floor ($E = E_{seafloor}$). These assumptions implied that, for the air blast and thermal radiation models, a ground and water impact of the same impact energy were equivalent. Nevertheless, the presence of a water column could attenuate the seismic shaking intensity and the ejecta released compared to a ground impact scenario.

2.1. Cratering

The crater formation was an intricate process to model because it involves various stages, such as shock wave propagation, excavation of the impact surface, and depression formation, among others [14,21]. To simplify, the process was divided into two stages. First was the formation of a transient crater, i.e., an unstable structure that cannot support itself, and its subsequent gravity-induced collapse; and second was the formation of the final crater. In [14], through the usage of scaling laws and empirical data, analytical relations were developed to express the crater's dimensions. The same relations were also later presented in [13]. The transient crater diameter is given by:

$$D_{tc} = 1.161 \left(\frac{\rho_i}{\rho_t}\right)^{1/3} L^{0.78} v_i^{0.44} g_0^{-0.22} \sin^{1/3}\theta \tag{3}$$

where ρ_t and ρ_i are the densities of the target and the impactor, respectively; L is the impactor's diameter, v_i is the impact velocity, θ is the angle of impact, and g_0 is the Earth's standard gravitational acceleration.

For impacts on liquid surfaces, the scalar 1.161 had to be changed to 1.365 (3). In terms of final crater diameter, the threshold between simple and complex craters was at 3.2 km. For simple craters, the final crater diameter, from rim to rim, was given by:

$$D_{fc} = 1.25 D_{tc} \tag{4}$$

For complex craters, when the transient crater was greater than 2.56 km, the following expression [14] was used to obtain the final crater diameter instead:

$$D_{fc} = 1.17 \frac{D_{tc}^{1.13}}{D_c^{0.13}} \tag{5}$$

where D_c was the threshold diameter between a simple and a complex crater. The depth for the transient crater in relation the original ground plane was given by:

$$d_{tc} = \frac{D_{tc}}{2\sqrt{2}} \tag{6}$$

The depth of the complex final crater, defined in [22], was expressed as:

$$d_{fc} = 0.294512 D_{fc}^{0.34013}. \tag{7}$$

For the simple crater, the depth was simply:

$$d_{fc} = d_{tc} + h_{fr} - t_{br} \tag{8}$$

where h_{fr} and t_{br} were, respectively, the rim height and the thickness of the breccia lens obtained by:

$$h_{fr} = 0.03584 D_{tc} \tag{9}$$

$$t_{br} = 0.123354 D_{tc} \tag{10}$$

Finally, the volume of the transient crater was:

$$V_{tc} = \frac{\pi D_{tc}^3}{16\sqrt{2}} \tag{11}$$

2.2. Seismic Shock

An asteroid impact event can create a seismic shock associated with the impactor's kinetic energy [23,24]. The Gutenberg–Richter magnitude energy relation, referenced in [14] and later in [13], provides the seismic magnitude of an impactor as a function of its kinetic energy:

$$M = 0.67 \log_{10} E - 5.87 \tag{12}$$

where E is the kinetic energy in Joules, and M is the seismic magnitude on the Richter scale. The seismic intensity decayes over the travelled distance. The effective magnitude M_{eff} of the seismic shock in a specific location, at a distance D from the epicentre, was expressed in [14] and later in [13] as:

$$M_{eff} = \begin{cases} M - 2.38 \times 10^{-5} D & : 1 \\ M - 4.8 \times 10^{-6} D - 1.1644 & : 2 \\ M - 1.66 \log_{10} \Delta - 6.399 & : 3 \end{cases} \tag{13}$$

For (13), case 1 was valid when D was less than 60 km, case 2 when D was less than 700 km and greater or equal than 60 km, and case 3 only for D values greater or equal than 700 km, where Δ was the angle, in radians, between the impact site and the location, defined in (20).

2.3. Air Blast

Like explosions, a widely studied field, asteroid impacts create shock waves that increase the atmospheric pressure at the vanguard [14,25]. The yield scaling distance D_1 that experiences the same peak overpressure as results from the explosion of 1 kt of TNT (trinitrotoluene, 1 TNT $= 4.184 \times 10^{12}$ J) can be found. The yield scaled distance D_1 is expressed as:

$$D_1 = \frac{D}{E_{kt}^{1/3}} \tag{14}$$

where D is the distance from the impact site and E_{kt} is the yield energy in kilotons TNT. The decay of the peak overpressure in Pa as a function of the yield scaled distance can be obtained by:

$$p_D = \frac{p_x D_x}{4D_1}\left(1 + 3\left[\frac{D_x}{D_1}\right]^{1.3}\right), \tag{15}$$

for which the values p_x and D_x were 75,000 Pa and 290 m, respectively, [14].

2.4. Thermal Radiation

In the surroundings of an impact site, a collision event drastically raises the temperature and pressure [14,26,27]. A method that evaluates and computes the thermal energy emanating from an impact event was presented in [13,14]. For impact velocities higher than 12 km/s, the shock pressure could melt the impactor and some target material; vaporisation occurs for velocities higher than 15 km/s. The vapour generated, named a fireball, has very high pressure and temperatures, and it expands rapidly. This thermal radiation model neglects the effects of atmospheric conditions and the variation in atmospheric absorption with altitude above the horizon. The empirical relation between the radius of the fireball R_f in meters and the impact energy E in Joules is given by:

$$R_f = 0.002E^{1/3} \tag{16}$$

Thermal radiation is only a fraction of the kinetic energy released during an impact. This fraction, the luminous efficiency η_{lum}, for asteroid impacts with Earth is in the range of $10^{-4} - 10^{-2}$, a range found through limited experimental and numerical results in [14]. The thermal energy per area unit was given by:

$$\phi = f\frac{\eta_{lum}E}{2\pi D^2} \tag{17}$$

where f was the fraction of a fireball visible over the horizon at distance D, obtained by:

$$f = \frac{2}{\pi}\left(\cos^{-1}\frac{h}{R_f} - \frac{h}{R_f}\sin\left[\cos^{-1}\frac{h}{R_f}\right]\right) \tag{18}$$

In (18), h was the maximum height of the fireball below the horizon at a distance D, and it was defined by:

$$h = (1 - \cos\Delta)R_E \tag{19}$$

where Δ was the angle defined by:

$$\Delta = \arccos[\sin\phi_i \sin\phi_k + \cos\phi_i \cos\phi_k \cos(|\lambda_i - \lambda_k|)] \tag{20}$$

Then, using (16), if $h \geq R_f$, the fireball was entirely below the horizon, which meant that there was no direct thermal radiation reaching the location defined by (20), disregarding the radiation deflection in the atmosphere.

2.5. Ejecta Material

The ejection of material from the impact site is one of the consequences of a solid ground collision. This ejected material, named ejecta, could endanger populations if landing directly in civilised areas: when a blanket of dense particles that covers the surroundings is formed; or when infrastructure is damaged, such as buildings or bridges, to the point of collapse by deposition; or by direct collision. In [14], analytical equations were deduced to estimate the mean ejecta fragment diameter and the ejecta blanket thickness that were

later exposed in [13]. The mean ejecta fragment diameter L_e, in meters, could be given, as a function of the final crater diameter D_{fc} and distance D, by:

$$L_e = 2400\left(\frac{D_{fc}}{2000}\right)^{-1.62}\left(\frac{D_{fc}}{2D}\right)^{2.65} \tag{21}$$

The ejecta blanket thickness t_e as a function of the transient crater diameter D_{tc} and the distance D is then:

$$t_e = \frac{D_{tc}^4}{112D^3} \tag{22}$$

2.6. Tsunami

An asteroid impacting water generates a circular wave pattern, like a droplet impacting a liquid film. The event causes the formation of two waves: rim waves and collapse waves. These waves could reach tremendous heights, hit inhabited coastal regions, and wreak havoc. The assessment was divided into two stages: the deep-water wave amplitude propagation and the wave run-up in shallow waters. The wave amplitude attenuation models estimated the evolution of the maximum wave amplitude in waters deeper than 800 m, where the benthic floor depth was assumed to remain constant and equal to the impact location. In shallow waters, given the wave amplitude at the threshold point, the model estimated the run-up evolution until the coast, where a positive constant slope for the ocean floor was assumed.

2.6.1. Rim Wave

The initial asteroid impact on the ocean surface would radially displace the water to create the transient surface crater. This displacement originated the wave perturbation that eventually developed into the first tsunami wave in the model, the rim wave. In [22], a propagation model was developed for the rim-wave amplitude. The models presented a $1/D$ wave decay with radial distance, which agreed with oceanic impact simulations [20]. The maximum rim-wave amplitude was:

$$A_{rw}^{max} = \min\left(\frac{D_{tc}}{14.1}, h_{sea}\right) \tag{23}$$

The rim-wave amplitude A_{rw} at a distance D from the impact location was:

$$A_{rw} = A_{rw}^{max}\left(\frac{3D_{tc}}{4D}\right) \tag{24}$$

2.6.2. Collapse Waves

The second type of wave is a product of the surface transient crater collapse. The impact-induced surface transient crater is filled by the adjacent ocean through centripetal inflow. The radial inflow creates a water peak at the centre of the then-collapsing crater that would continue to oscillate radially in and out until all energy is dissipated. Each oscillation generates a collapse wave. In the present model, the formation of the collapse wave is assumed to be unique and unrepeatable. In [22], a model to predict the collapse wave amplitude decay over the distance was defined. The maximum collapse wave amplitude was given by:

$$A_{cw}^{max} = 0.06\ min\left(\frac{D_{tc}}{2.828}, h_{sea}\right) \tag{25}$$

The collapse wave amplitude decay as a function of the distance D was defined as:

$$A_{cw} = A_{cw}^{max}\left(\frac{5D_{tc}}{2D}\right)^{q} \tag{26}$$

where q was the attenuation factor, defined as:

$$q = 3e^{-0.8L/h_{sea}} \text{ for } L/h_{sea} < 0.5 \tag{27}$$

2.6.3. Run-Up

The wave run-up U is the maximum height the wave can reach, i.e., the maximum vertical extent of a wave, given the slope s of the coastal region. In [13], a simple analytical model was developed to assess the run-up estimation U, which uses the following expression for its computation:

$$U = 2sA_{800}\left(\frac{A_{800}}{D_{tc}}\right)^{-0.5} \tag{28}$$

where A_{800} is the wave's amplitude when it reaches shallow water, defined as being depths less than 800 m. The shore slope s is simply defined by the commonly known rise over run formula:

$$s = \frac{|h_{800} - h_k|}{D_{shore}} \tag{29}$$

where D_{shore} is the distance from the 800 m depth point to the location, h_{800} is per definition -800 m, and h_k is the location's altitude.

For every location, the maximum and minimum slopes were obtained by inserting the maximum $h_{k_{max}}$ and minimum $h_{k_{min}}$ altitude in (29). With these two new variables, the maximum run-up U_{max} and the minimum run-up U_{max} were computed. However, even if the slope considers the elevation of the location, the run-up is in relation to the sea level. Thus, a local run-up U_l was assessed in which the minimum altitude of the location was:

$$U_l = U - h_{k_{min}} \tag{30}$$

This local run-up could be defined as the run-up resulting in the maximum local run-up, or on the other hand, in the minimum run-up.

2.7. Global Effects

In [14], a simple way to assess the global effect was presented: computing the linear and angular momentum ratios between the Earth and the impactor, and the volume ratio of the transient crater diameter and the Earth's volume.

The linear momentum of the impactor M_i could be obtained by relating its mass m_i and its impact velocity v_i:

$$M_i = m_i v_i \tag{31}$$

Earth's linear momentum was obtained in a similar way while assuming its mass as $m_E = 5.83 \times 10^{24}$ kg and its mean orbital velocity as v_E = 29,780 m·s^{-1}. The angular momentum of the impactor was obtained by:

$$\Gamma_i = m_i v_i R_E \cos\theta. \tag{32}$$

The Earth's angular momentum was assumed to be Γ_E = 5.86 $\times$ 10^{33} kg·m^3·s^{-1}. The volume of the Earth was obtained assuming a 6371 km radius sphere. Depending on the three ratios mentioned, the qualitative global implications of the impact could be observed in Table 1.

The variation in the Earth's rotation period ΔT_E can be obtained using the asteroid's mass m_i, velocity v_i, and impact angle θ; and Earth's radius R_E, mass M_E, and rotation period T_E [22]:

$$\Delta T_E = \frac{5}{4\pi R_E}\frac{m_i}{M_E}\cos\theta\, v_i T_E^2 \tag{33}$$

Table 1. Global implications of an impact event [14].

Ratio	Interval	Qualitative Global Change
M_i/M_E	$[-\infty; 0.001]$	No noticeable change in orbit.
	$[0.001; 0.01]$	Noticeable change in orbit.
	$[0.01; 0.1]$	Substantial change in orbit.
	$[0.1; +\infty]$	Totally changes orbit.
Γ_i/Γ_E	$[-\infty; 0.01]$	No noticeable change in rotation period and tilt of axis.
	$[0.01; 0.1]$	Noticeable change in rotation period and tilt of axis.
	$[0.1; 1.0]$	Substantial change in rotation period and tilt of axis.
	$[1.0; +\infty]$	Totally changes rotation period and tilt of axis.
V_{tc}/V_E	$[-\infty; 0.1]$	Earth is not strongly disturbed and loses negligible mass.
	$[0.1; 0.5]$	Earth is strongly disrupted but loses a little mass.
	$[0.5; +\infty]$	Earth is completely disrupted and loses all mass.

2.8. Vulnerability

The vulnerability models we used estimate the ratio of the population lethally harmed by an asteroid impact. Vulnerability is intrinsically related to the severity of the impact effects, which is a function of the distance. Our models did not consider the time of day in which the impact event occurs. They did not consider the terrain orography, the meteorological conditions, or the wind's direction. The populations were also assumed to have no previous warning about the threat. They were also independent of one another; i.e., the total vulnerability of a given location was not the sum of every individual effect's vulnerabilities.

2.8.1. Seismic Shaking

To properly relate the seismic shaking intensity with the mortality rate in [28], a literature review was conducted to collect relevant data and deduce a seismic shaking vulnerability model. The variability in the vulnerability dataset was ample, allowing the establishment of best, worst, and expected scenarios. The equation relates the seismic magnitude on the Richter scale, of a given place, with the population's vulnerability to that event. The equation representing the three cases is:

$$V_{\text{seis}} = \frac{1}{1 + e^{a\left(M_{eff} + b\right)}} \tag{34}$$

where a and b are coefficients defined in Table 2 for each one of the three cases: best, expected, and worst-case scenarios. All vulnerability models are represented graphically in Figure 1a.

Table 2. Seismic shaking vulnerability coefficients.

	a	b
best	−2.51	−9.59
expected	−2.52	−8.69
worst	−3.80	−7.60

2.8.2. Overpressure

High internal–external body pressure differentials endanger people. To extrapolate the vulnerability models, data that provided information about non-lethal, half-lethal, and entirely lethal pressure differentials were utilised [28]. With the bounding pressure values for each measure, best, worst, and expected pressure vulnerability models were developed. However, these did not consider the damage done to infrastructure and its

potential effect on the population. In Figure 1b, the vulnerability cases and the data are presented. The vulnerability models as logistic functions were as follows:

$$V_{\mathrm{p}} = \frac{1}{1 + e^{a(p+b)}} \tag{35}$$

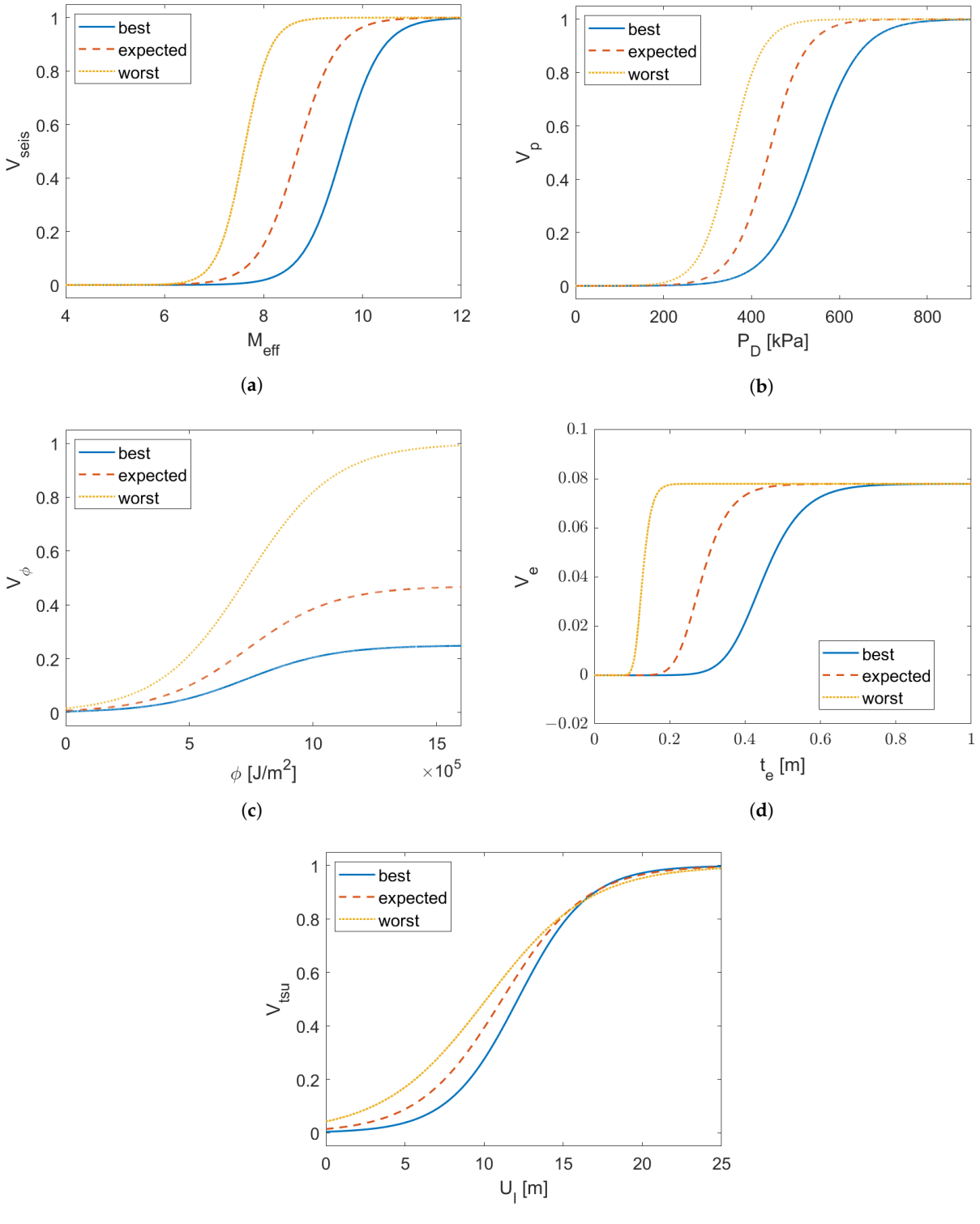

Figure 1. Best, worst, and expected-case vulnerability models. (**a**) Seismic shaking. (**b**) Overpressure. (**c**) Thermal radiation. (**d**) Ejecta blanket deposition. (**e**) Tsunami.

The coefficients a and b are defined in Table 3. In Figure 1b, the three overpressure vulnerability scenarios are represented graphically.

Table 3. Overpressure vulnerability coefficients.

	$a \times 10^5$	$b \times 10^{-5}$
best	−1.90	−5.43
expected	−2.42	−4.40
worst	−2.85	−3.53

2.8.3. Thermal Radiation

Thermal radiation could burn or ignite a surface that it encounters. This can include the skin, and therefore, thermal radiation could be fatal. In [28], different kinds of relevant data were assembled to develop a thermal radiation vulnerability model. These data included the skin burn probability, the burn degree distribution as a function of the radiation exposure, and the mortality rates of treated and untreated burn victims as functions of burnt total body surface area. To obtain the mortality rate as a function of radiant exposure, the authors also considered that clothes offer some protection and that only one side of a person was exposed to radiation. Finally, to develop the different cases' vulnerability models, the authors considered the global unsheltered population at any given moment. For the best-case scenario, all the population was sheltered, but 25% were affected via windows. For the expected case, the authors assumed an unsheltered population of 47%. In the worst-case scenario, all the population was assumed to be exposed. The vulnerability model was given by:

$$V_\phi = \frac{a}{1 + e^{b(\phi + c)}} \tag{36}$$

Table 4 presents the respective coefficients.

Table 4. Thermal radiation vulnerability coefficients.

	a	$b \times 10^6$	$c \times 10^{-5}$
best	0.25	−5.62	−7.32
expected	0.47	−5.62	−7.32
worst	1.00	−5.62	−7.32

Figure 1c shows all three thermal exposure vulnerability models, the best, expected, and worst-case scenarios.

2.8.4. Ejecta Blanket Deposition

The ejected material from the cratering process threatens the populations because its deposition could lead to the collapse of buildings because of the ejecta blanket weight load. The ejecta could also bludgeon individuals and cause fatalities. Nonetheless, the vulnerability model only included the former peril. A model that related the ejecta blanket thickness t_e and its vulnerability was developed in [28]. The authors assumed a mean ejecta material density ρ_e of 1600 kg·m^{-3} to assess the load of the ejecta blanket, given by:

$$p_e = t_e \rho_e g_0 \tag{37}$$

The authors also assumed that 78% of the affected population was indoors. Furthermore, 20% of occupants of a given house would be trapped inside, given a collapse, and 50% of those trapped would be killed. In a roof collapse event, the maximum population vulnerability was $0.78 \times 0.2 \times 0.5 = 0.078$. The likelihood of this event was modelled considering the ejecta load and the building's strength. Therefore, the best, expected, and worst-case

scenarios derive from different building strengths. The sigmoid obtained through the preceding approaches is:

$$V_e = \frac{0.078}{\left[1 + e^{a(p_e+b)}\right]^c} \tag{38}$$

where the ejecta load p_e is in kPa. In turn, the coefficients a, b, and c varied depending on the scenario presented in Table 5. Figure 1d represents all three vulnerability cases.

Table 5. Ejecta blanket deposition vulnerability coefficients.

	a	b	c
best	−1.00	−5.84	−2.58
expected	−1.37	−3.14	−4.60
worst	−4.32	−1.61	−4.13

2.8.5. Tsunami

A large body of water in a waveform could be devastating when hitting an inhabited coastal region. The aftermath of a tsunami is no easy task to assess because its high complexity and dependence on various external factors. In [28], a simple analytical approach was developed to analyse a tsunami wave and its subsequent fatalities. The tsunami vulnerability was obtained as a function of the local run-up U_l, which varied according to the scenario, Table 6. The relation was:

$$V_{tsu} = \frac{1}{1 + e^{a(U_l+b)}}. \tag{39}$$

Its coefficients are defined in Table 6, and the visual representation is in Figure 1e.

Table 6. Tsunami vulnerability coefficients.

	$a \times 10^1$	$b \times 10^{-1}$	U_l
best	−4.53	−1.21	$U_{min} - h_{k_{min}}$
expected	−3.80	−1.11	$U_{min} + U_{max}/2 - h_{k_{min}}$
worst	−3.07	−1.02	$U_{max} - h_{k_{min}}$

3. Results and Discussion

Using three sets of coordinates to represent mainland Portugal, Azores, and Madeira, the midpoint or impact location had latitude and longitude of 39.6177° N and 16.9532° W, respectively. The impact effects depend heavily on the distance travelled by the impact effect. Thus, utilising single points to represent mainland Portugal, the Azores, and Madeira Islands is highly inaccurate. Therefore, the impact effects assessment was performed for all 308 Portuguese municipalities, considering each distance to the impact site. However, to not over-complicate the exposition, the intensity of the impact effects is only shown for the closest point to the impact site on each of mainland Portugal, Azores, and Madeira. The casualties represent the individual municipality casualties' sums; e.g., the pressure casualties attributed to Portugal represent the pressure casualties of all Portuguese municipalities on the continent. The points that represent groups in the three territories correspond to the Portuguese municipalities of Peniche for mainland Portugal, Nordeste for Azores island, and Porto Santo for Madeira island. Table 7 displays the physical data of the asteroids.

3.1. Cratering

The crater dimensions of all impacts with the ocean surface and ocean seafloor were obtained via Equations (3)–(11) for the three asteroids, rather than modelling. Both surface and sea floor final craters created by Apophis are simple. The respective theoretical visual representations can be seen in Figures 2–4.

Table 7. Asteroids' physical and impact properties.

		L [m]	θ [°]	ρ_i [kg/m^3]	v_i [m/s]	E [J]
Apophis	surface sea floor	370	45	3200	12,620 5.6	6.8×10^{18} 1.3×10^{12}
Medium Asteroid	surface sea floor	204	45	3100	10,840 5.8×10^{-3}	8.1×10^{17} 2.3×10^{5}
5 km Impactor	surface sea floor	5000	45	2500	15,000 7.2×10^{3}	1.8×10^{22} 4.3×10^{21}

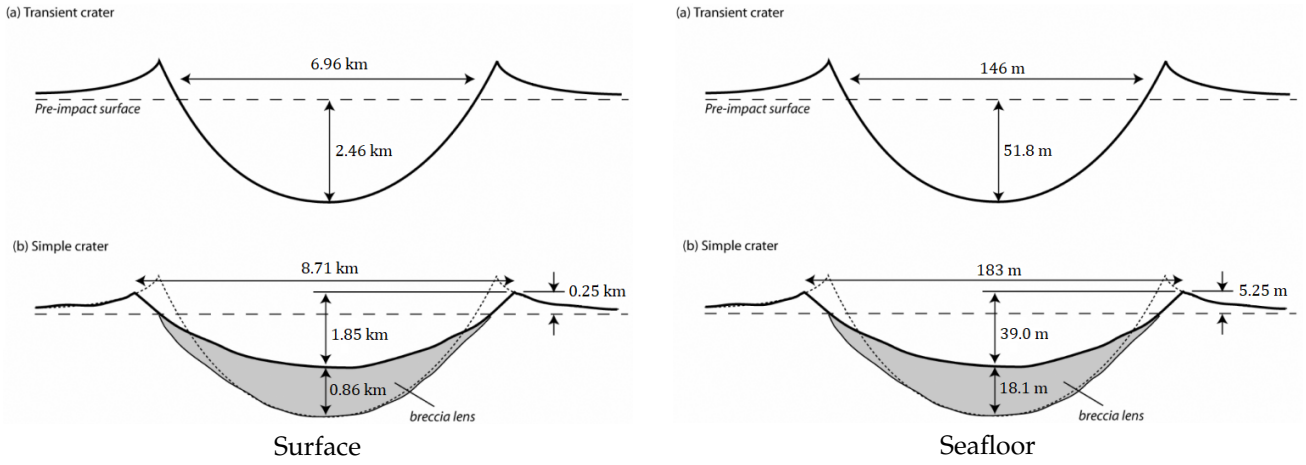

Figure 2. Apophis crater dimensions for the transient craters (**a**) and the simple final craters (**b**) for the surface and sea floor were obtained by the listed relations (3)–(11) rather than modelling.

The impact velocity on the sea floor is attenuated about eight orders of magnitude because of the presence of the water layer, rendering the final impact velocity on the benthic layer negligible. Despite this, the dimensions of both surface and sea floor medium-asteroid-generated craters can be seen visually in Figure 3.

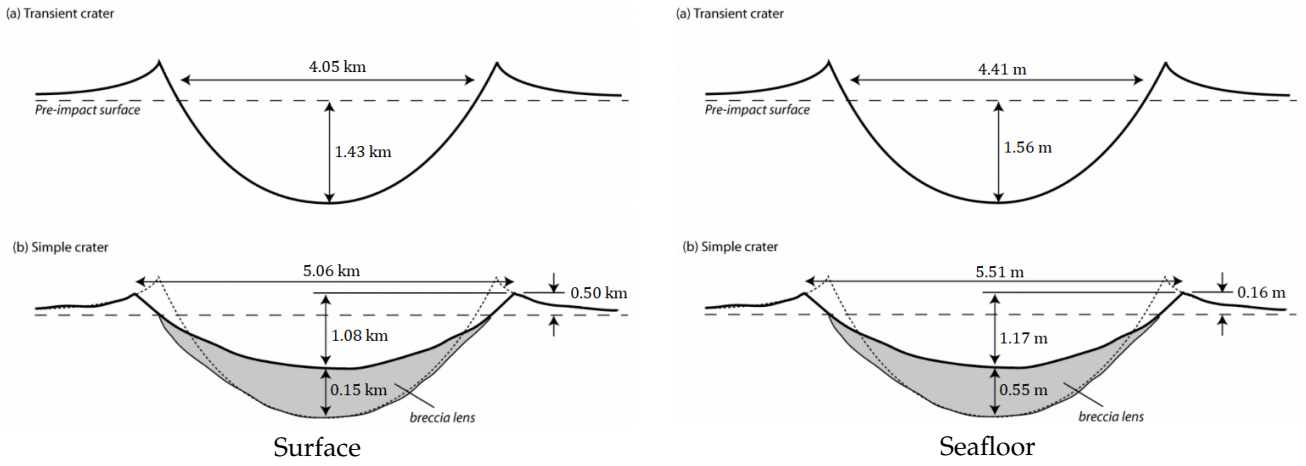

Figure 3. Medium asteroid crater dimensions for the transient craters (**a**) and simple final craters (**b**) on the surface and sea floor were obtained by the listed relations (3)–(11) rather than modelling.

The 5 km asteroid's transient crater penetrates the ocean 4.91 km deep. The almost one-to-one relationship between the diameter and ocean depth suggests that the water layer is not a significant factor in attenuating the impact. With a ratio of 0.982 between the depth and diameter, the impact corresponds to a shallow water impact [20]. In shallow waters, some authors consider the formation of a single crater on the sea floor because of

the minor difference between the water depth and the asteroid's diameter [20]. However, in this paper, the formation of both theoretical craters is considered. In Figure 4, said craters' dimensions can be seen.

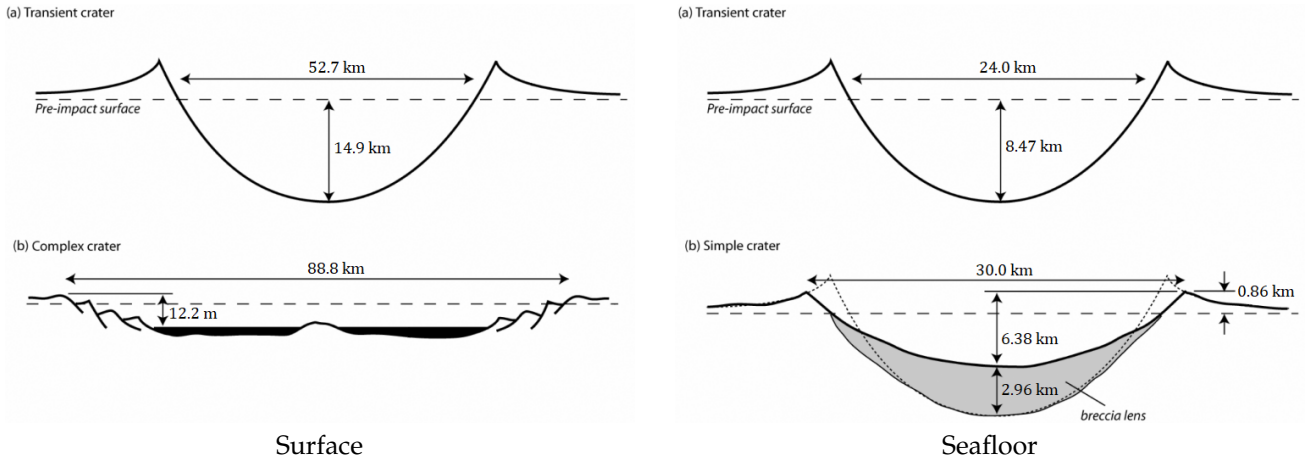

Figure 4. Five-kilometre asteroid impactor crater dimensions for the transient craters (**a**) and simple final craters (**b**) on the surface and sea floor were obtained by the listed relations (3)–(11) rather than modelling.

The 5 km impactor's transient crater spans a massive 52.7 km from rim to rim, alluding to the potential damage to the landscape and population if such an impact occurs in a densely populated area. The crater's depth is three times the ocean's depth, which is impossible without benthic strata excavation, which refers to its theoretical nature.

3.2. Seismic Shaking

The absolute magnitude M in (12), the Richter magnitude value at the epicentre, is a direct function of the impact energy E. The effective magnitude M_{eff}, Equation (13), is the Richter magnitude value attenuated by the distance D to the epicentre, in this case, the impact site.

The seismic shaking caused by the Apophis impact has an absolute magnitude of 2.3 on the Richter scale. The impact velocity on the sea floor is reduced by four orders of magnitude, compared to the surface impact velocity, because of the presence of the water layer, which significantly decreases the impact energy and the seismic shaking magnitude. Table 8 lists the distance D and the effective magnitude M_{eff} of the seismic shaking for three Portuguese locations. Figure 5a graphically represents the effective magnitude M_{eff} for all studied municipalities as a function of the impact site distance D. The seismic shaking model allows for negative values. The negative values have no physical representations. They merely mean that the effect does not reach that location.

The impact of the medium asteroid into the ocean floor would induce a seismic shaking of magnitude $M = -2.3$. This value is purely theoretical and means that the collision does not create a seismic wave. The non-existing seismic wave, because of the asteroid reaching the sea floor at such a low velocity, corroborates the possibility of disregarding the ocean floor impact completely. Nevertheless, Table 8 displays the effective magnitudes for the three locations, and Figure 5a for all municipalities.

The 5 km impactor's sea floor impact generates a seismic shaking of $M = 8.62$ on the Richter scale. This event can be loosely compared to the 8.4 Lisbon earthquake of 1755 in terms of absolute magnitude, even though the distance between mainland Portugal and the epicentral point was roughly 300 km, less than half the distance D between mainland Portugal and the impact location. Distance plays a huge role in attenuating the seismic waves. As can be seen in Table 8 and in Figure 5a, most municipalities would experience an effective magnitude M_{eff} of around 3.8, less than half the absolute value. By consulting the Abbreviated Modified Mercalli Intensity scale [14], we can convert these average

magnitudes into qualitative terms. In the Mercalli scale, the correspondent intensities are III and IV.

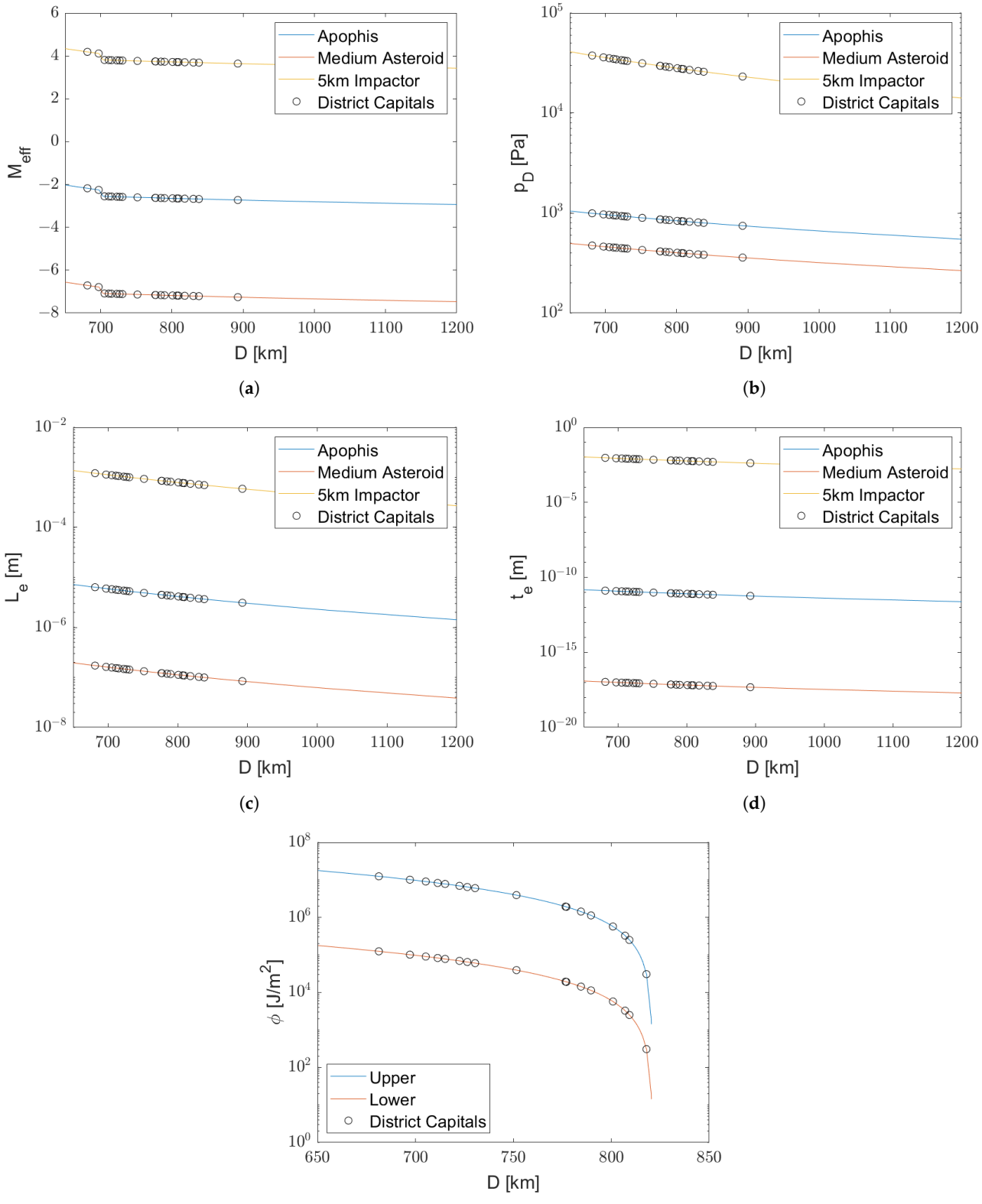

Figure 5. Impact effects as functions of the municipalities' distances. The trends are represented by continuous lines. (**a**) Effective magnitude. (**b**) Overpressure. (**c**) Mean ejecta fragment diameter. (**d**) Ejecta blanket thickness. (**e**) Upper and lower thermal radiation.

Table 8. Impact effects in Portuguese territory.

		D [km]	M_{eff}	D_1 [km/kt$^{-1/3}$]	P_D [kPa]	h/R_f	ϕ^- [kJ/m^2]	ϕ^+ [kJ/m^2]
1	Mainland	650.3	−2.0	5.5	1.0	8.8	0	0
	Azores	737.6	−2.6	6.3	0.9	11	0	0
	Madeira	731.2	−2.6	6.2	0.9	11	0	0
2	Mainland	650.3	−6.6	11	0.5	18	0	0
	Azores	737.6	−7.1	13	0.4	23	0	0
	Madeira	731.2	−7.1	13	0.4	23	0	0
3	Mainland	650.3	4.3	0.4	41	0.6	1.8×10^2	1.8×10^4
	Azores	737.6	3.8	0.5	33	0.8	5.3×10^1	5.3×10^3
	Madeira	731.2	3.8	0.4	33	0.8	6.0×10^1	6.0×10^3

3.3. Overpressure

The overpressure values from the impact-induced shock wave were obtained with (15). The distance D_1 in (14) is the distance to a 1 MT TNT equivalent explosion that experiences the same overpressure effects as the distance D from impact energy E. Both the distance D_1 and the pressure P_D, for each impact scenario, are shown in Table 8. Figure 5b displays the overpressure P_D as a function of the distance D for the three asteroids.

The Apophis-induced pressure values are in the high hundreds/low thousands, only potentially shattering windows, which requires 6.90 kPa. In the medium-asteroid scenario, the overpressure values lie in the mid-hundreds range, not even allowing them to destroy windows.

For the 5 km impactor, the pressure results for all studied municipalities are naturally higher. Despite the results being in the several hundreds of pascals, the pressure difference would be felt, but not with significant consequences to the population directly. Most locations would experience the shattering of glass windows (6.90 kPa), the roofs would be severely damaged (22.9 kPa), and wood-framed buildings would almost collapse completely (26.8 kPa). In the most affected locations, multi-story wall-bearing buildings would experience severe cracking, and interior partitions could be blown down (38.5 kPa) [14].

3.4. Thermal Radiation

The thermal radiation assessment demands the estimation of the fireball generated, obtained with (16). Any other energy transfer method, such as atmospheric reflection, was dismissed. Two fractions related to the percentile of exposure of any location, because to the curvature of the Earth, needed to be estimated to determine the radiation that reaches a given municipality. The first was the ratio between the maximum fireball height below the horizon and the fireball radius h/R_f. The second one was the fraction of visible fireball over the horizon f, defined in (18). Both are intrinsically related: if $h/R_f > 1$, then $f = 0$, and the municipality is completely shielded from direct exposure; if $0 < h/R_f < 1$, then $0 < f < 1$, meaning the location is exposed to thermal radiation, but has some protection; if $h/R_f = 0$, then $f = 1$, and the location is completely exposed, making Earth's curvature irrelevant. The luminous efficiency needs to be defined to complete the assessment and estimate the thermal radiation per location. This value is the fraction of kinetic energy converted into thermal radiation. We set the upper ϕ^+ and lower ϕ^- thermal radiation limits to 10^{-4} and 10^{-2} in the present work.

In Table 8, we can see the ratio of the maximum fireball height below the horizon to the radius of the fireball $h = R_f$, and the high and low thermal radiation bounds ϕ, for the Portuguese territory. For the impact scenarios of Apophis and the medium asteroid, rows 1 and 2, respectively, all the $h = R_f$ values surpass unity. The locations are shielded from direct exposure, thereby not experiencing thermal radiation. Since every location has a zero joule per square metre thermal exposure, the vulnerabilities and casualties associated with this impact effect are also zero.

For the 5 km impactor scenario, row 3, the difference between upper and lower thermal radiation is two complete orders of magnitude for any studied municipality. The difference is related to the luminous efficiency, as the limits of the fraction also vary by two orders of magnitude. Figure 5e visually represents the upper and lower thermal radiation. From a distance of $D = 820.9$ km onwards, no thermal radiation is experienced. For any municipality with a higher distance value, the fraction $h = R_f$ is more than one, and all subsequent values are zero.

Given the thermal radiation values for any given location, the qualitative impact effects can be estimated by comparison with the ignition factors of various materials. Assuming the highest thermal radiation ϕ^+ possible, mainland Portugal and the Azores would experience the burning of clothes, plywood, grass, newspaper, and deciduous trees, and third-degree burns; see Table 1 from reference [14]. The Madeira Islands would experience the burning of grass, newspapers, and deciduous trees, while the population would experience second-degree burns. Assuming the lower thermal radiation ϕ^-, the population would not experience first degree burns, and no materials would ignite.

3.5. Ejecta

The material ejected from the crater is simpler to assess. Both the mean ejecta fragment diameter L_e and the ejecta blanket thickness t_e can be obtained by the direct relations presented in (21) and (22), respectively. The ejecta vulnerability assessment uses the ejecta blanket thickness t_e, which, according to Figure 1d, should be in the centimetre range to have an impact on the population. In Table 9, both variables are shown for the three simulated impacts. In Figure 5c,d these values are represented visually for all studied municipalities.

Table 9. Ejected material for the closest impact point in mainland Portugal, Azores and Madeira.

	Apophis		**Medium Asteroid**		**5 km Impactor**	
	L_e **[µm]**	t_e **[pm]**	L_e **[nm]**	t_e **[am]**	L_e **[mm]**	t_e **[mm]**
Mainland	7.2	14.9	195	12.3	1.4	10.7
Azores	5.1	10.2	139	8.4	0.98	7.3
Madeira	5.3	10.5	143	8.6	1.0	7.5

For the Apophis impact, the ejected material from the collision site, either the mean diameter of ejecta fragments L_e or the ejecta blanket deposition t_e, would not be significant in size. The former would be in the range of micrometres and the latter in picometres. These values are too small to be perceived by the population and are likely to not cause any concerning damage, resulting in values of vulnerability and casualties of zero.

For the medium-asteroid scenario, the ranges of the mean ejecta fragment diameter L_e and the ejecta blanket thickness t_e are in nanometres and attometres. Therefore, the vulnerabilities and casualties would most likely be zero.

For the 5 km impactor, the mean ejecta fragment diameter L_e and the ejecta blanket thickness t_e would be in the millimetre range, making the matter perceivable by the population. The model did not assess the upper limit of mean ejecta fragment diameter, and larger chunks could still harm the population.

3.6. Tsunami

The ocean depth at the impact location is 4.91 km. Thus, the ratio L_0/h_{sea} defines Apophis and the medium asteroid's impacts as deep-water impacts, and the tsunami wave analysis consisted of two wave amplitude decay methods: one rim-wave amplitude method and one collapse wave amplitude method (Figure 6).

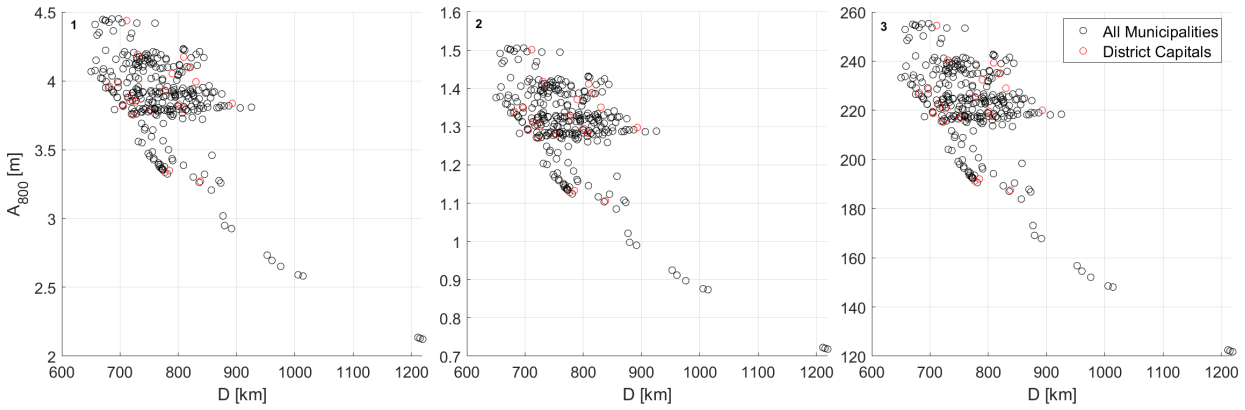

(**a**)

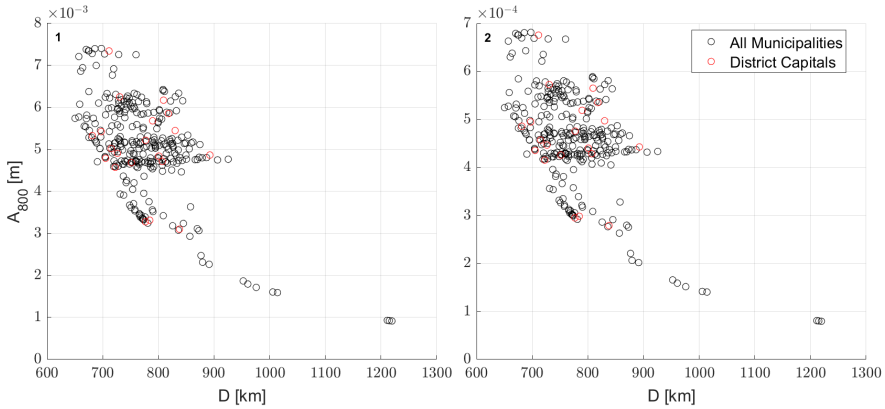

(**b**)

Figure 6. Tsunami wave amplitudes for Apophis (1), the medium asteroid (2), and the 5 km impactor (3) at 800 m depth as functions of the distance to municipalities. The black circles represent all municipalities. The red markers represent the values for the district capitals. (**a**) Rim-wave amplitude. (**b**) Collapse wave amplitude.

The 5 km impactor collision event is considered a shallow-water impact because of the asteroid diameter to ocean depth ratio L_0/h_{sea}. For such scenarios, a collapse wave would not form, and the only tsunami threat would be the creation and propagation of the rim wave [20]. Therefore, the tsunami assessment disregarded the formation of the collapse wave.

The wave amplitude propagation method disregards the ocean bathymetry, despite its relevance. The threshold between shallow and deep waters lies at the 800-m depth point, giving it extra significance [13]. Since the waters near the coast are less than 800 m deep and considered shallow, the amplitude method is not valid. Therefore, the authors developed a run-up wave computation method to properly assess the evolution of the waves near the coast and their final journey to the coastline. Figure 6 represents the tsunami waves amplitude at the threshold point obtained through (24) and (26).

The principal variable in the tsunami hazard assessment is the run-up wave at the coastline. Thus, the paramount concern of the estimation is the wave behaviour in shallow water. To assess the run-up wave height, i.e., the height the wave can reach inland, the wave amplitude at the 800-m point A_{800} and the distance from this point to the shore D_{shore} are needed. The value obtained with (28) cannot be directly used in the vulnerability models, as it assumes the location in question is at sea level. Since most of the studied municipalities are not coastal, a local run-up was calculated considering the maximum and minimum altitude. PORDATA, a contemporary Portugal geography database [29], provided the needed altitudes. The EDMOnet grid, which presents a detailed bathymetry profile of the European seas [30], supplied the D_{shore} values.

In Table 10, the most relevant values for the tsunami assessment are displayed. Row 1 represents the Apophis impact scenario, and rows 2 and 3 represent the medium-asteroid scenario and the 5 km impactor scenario, respectively. The amplitude at the deep–shallow water threshold, along with the corresponding minimum and maximum run-up, are presented for both waves. For rim-wave assessment, the amplitude values entail few disparities. The values only diverge in the run-up assessment. From this observation, the impact energy dictates the absolute nature of the values considered: amplitude and run-up, and the different slopes dictate the run-up fluctuation. The Azores and Madeira Islands present higher run-up values, possibly resulting from their volcanic nature and the reduced continental shelf that protects the coast of mainland Portugal.

In Figures 7a and 8a, there is a side-by-side comparison of the minimum and maximum run-up that the rim-wave amplitude method generates for the three impacts. All these run-up values are in relation to the sea level. The altitude still needs to be considered to obtain the local run-up.

The second wave amplitude decay method simulated is the one represented in (26), which tries to model the wave amplitude attenuation of the collapse wave with the distance. Table 10 displays these amplitude values. The relation between the amplitude and run-up values is similar to that in the previously discussed model. However, for the collapse wave, the orders of magnitude of the amplitude and run-up are lower than in the rim-wave estimations.

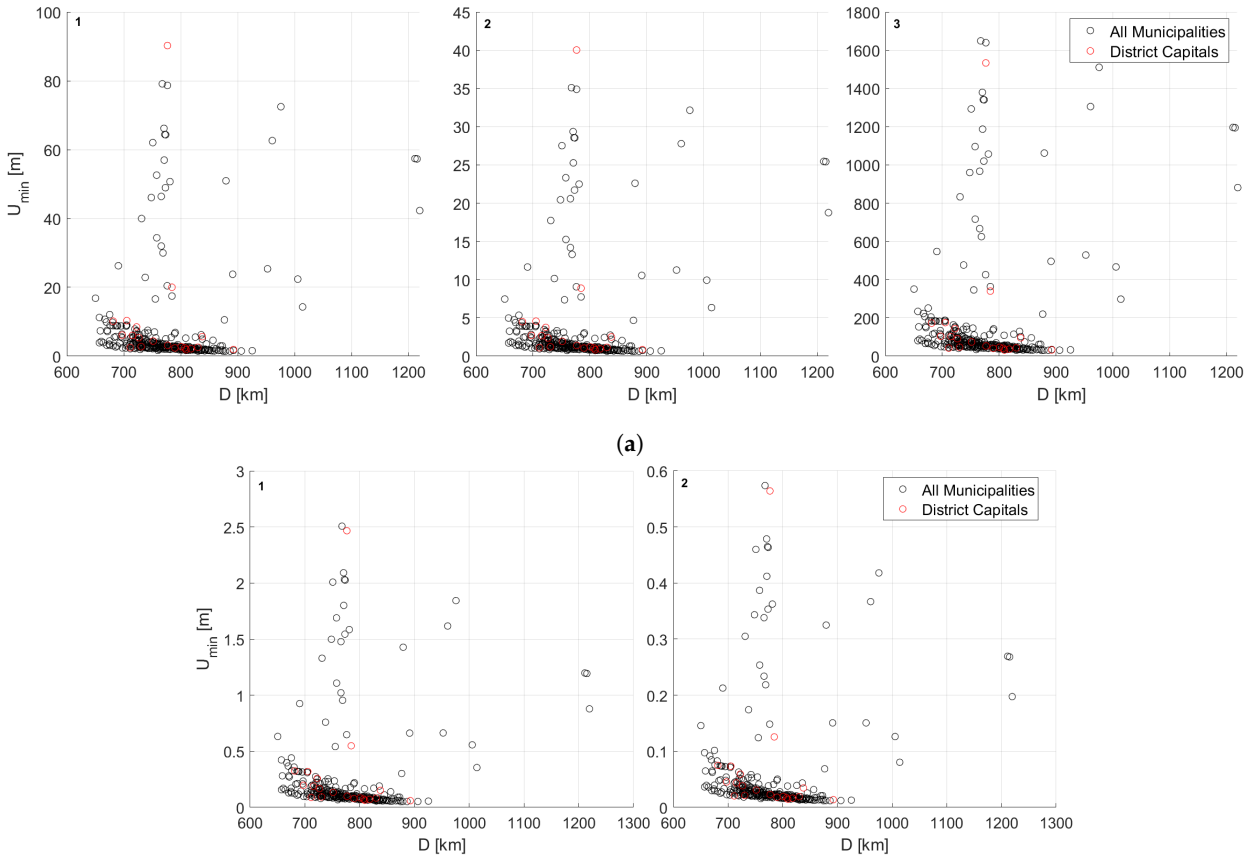

(**a**)

(**b**)

Figure 7. Tsunami wave minimum run-up for Apophis (1), medium asteroid (2), and 5 km impactor (3) impacts, at the coast, as functions of the distance to municipalities. The red markers represent the values for the district capitals. (**a**) Rim-wave. (**b**) Collapse wave.

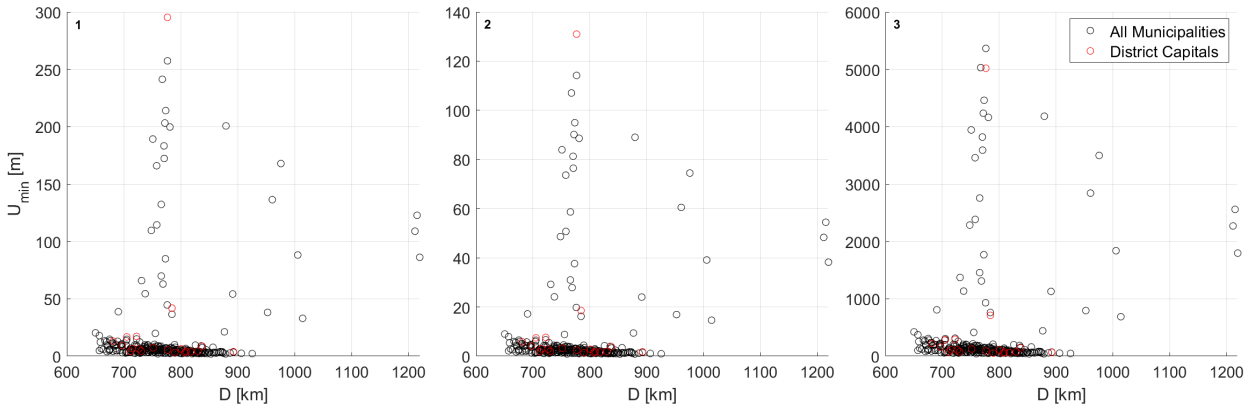

(**a**)

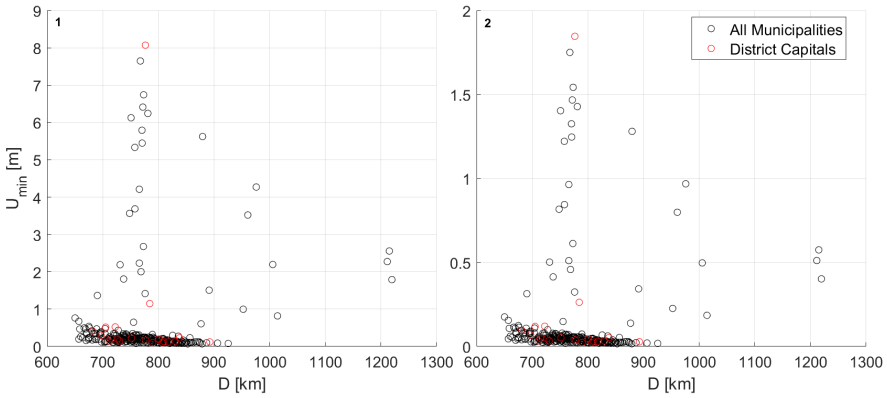

(**b**)

Figure 8. Tsunami wave maximum run-up for Apophis (1), medium asteroid (2), and 5 km impactor (3) impacts, at the coast, as functions of the distance to municipalities. The red markers represent the values for the district capitals. (**a**) Rim-wave. (**b**) Collapse wave.

The minimum and maximum run-up are represented in Figures 7b and 8b. Most of the values are inferior to one metre, resulting in low vulnerability. The results show a lesser threat from a collapse wave compared to a rim wave.

Table 10. Distance to the shore from the 800 m depth point, wave amplitude at this point, and run-up heights for the rim and collapse waves in Portuguese territory.

			Rim-Wave			**Collapse Wave**		
		D_{shore} [km]	A_{800} [m]	U^- [m]	U^+ [m]	A_{800} [mm]	U^- [m]	U^+ [m]
1	Mainland	16	4.1	17	20	5.7	0.6	0.8
	Azores	11	3.6	23	54	4.0	0.8	1.8
	Madeira	6.3	3.6	40	66	4.0	1.3	2.2
2	Mainland	16	1.4	7.5	9.0	0.5	15	18
	Azores	11	1.2	10	24	0.4	17	41
	Madeira	6.3	1.2	18	29	0.4	31	50
3	Mainland	16	2.3×10^2	3.5×10^2	4.2×10^2	—		
	Azores	11	2.0×10^2	4.8×10^2	1.1×10^3			
	Madeira	6.3	2.0×10^2	8.3×10^2	1.4×10^3			

3.7. Global Effects

Table 11 exposes the qualitative global implications of each impact studied. Row 1 represents the Apophis impact; row 2 represents the medium-asteroid impact, and row 3 represents the 5 km impactor. Apophis would change the length of the day on Earth by about 27 picoseconds, which would be imperceptible by the population. The medium-asteroid impact would change the length of the day on Earth by about 4.5 femtoseconds. As both asteroids have relatively small diameters and would impact Earth with relatively low velocities, their qualitative global implications are negligible. The 5 km impactor collision event would induce a 67 microsecond change in the total length of the day. That is a perceptible order of magnitude, but it is comparatively small. Even though this impact scenario would generate significant impact effects, they would not be on a large enough scale to cause any global change in the Earth's orbit, rotation period, tilt of the axis, or mass.

Table 11. Global implications of the three impact events.

	Ratio	Value	Qualitative Global Change
1	M_i/M_E	1.5×10^{-11}	No noticeable change in orbit.
	Γ_i/Γ_E	1.9×10^{-09}	No noticeable change in rotation period and tilt of axis.
	V_{tc}/V_E	1.8×10^{-09}	Earth is not strongly disturbed and loses negligible mass.
2	M_i/M_E	1.5×10^{-11}	No noticeable change in orbit.
	Γ_i/Γ_E	1.9×10^{-09}	No noticeable change in rotation period and tilt of axis.
	V_{tc}/V_E	1.8×10^{-09}	Earth is not strongly disturbed and loses negligible mass.
3	M_i/M_E	1.5×10^{-11}	No noticeable change in orbit.
	Γ_i/Γ_E	1.9×10^{-09}	No noticeable change in rotation period and tilt of axis.
	V_{tc}/V_E	1.8×10^{-09}	Earth is not strongly disturbed and loses negligible mass.

3.8. Vulnerability

This subsection displays the individual vulnerabilities and respective casualties for each impact effect. It is worth reiterating that the vulnerabilities and casualties presented in this section are independent of one another. Thus, the total casualties from an impact are not the sum of the individual effects' casualties.

The seismic shaking vulnerabilities were divided into three case scenarios, best, expected, and worst. For each, vulnerability V_{seis} and subsequent casualties C_{seis} were computed.

As seen in Table 8, the effective magnitude because of the Apophis' impact is negative, which is only a mathematical result and represents non-existent seismic shaking activity in that location. As there is no activity, the vulnerabilities and the casualties are zero.

The seismic shaking vulnerability results of the medium asteroid are clear, whether there is a sea floor impact or not. In any case, the vulnerabilities are zero. If we assume an impact, the extremely low velocity with which the asteroid would reach the benthic layer would result in a purely mathematical negative value for the absolute magnitude of seismic shaking. Therefore, the formation of seismic waves would not occur. On the other hand, if we assume from the beginning that the water layer completely absorbs the impact, the asteroid will not reach the sea floor and thus not create a seismic shaking event.

In Table 12, all three scenarios are shown for the 5 km impactor collision event. Even though the seismic shaking on the Richter scale is positive, this vulnerability model predicts almost zero casualties for seismic shaking of this scale.

Table 12. Seismic vulnerabilities and casualties in Portuguese territory.

	Best		**Expected**		**Worst**	
	C_{seis}	V_{seis}	C_{seis}	V_{seis} $[10^{-7}]$	C_{seis}	V_{seis} $[10^{-6}]$
Mainland	0	0	2	2.1	31	3.2
Azores	0	0	0	0	0	0
Madeira	0	0	0	0	0	0

The overpressure vulnerability model is divided into three case scenarios: best, expected, and worst. Each scenario is associated with a specific overpressure vulnerability V_p and a subsequent casualties value C_p. Table 13 depicts the vulnerabilities and casualties. The air blast's causalities for the Apophis and medium-asteroid scenarios, rows 1 and 2, despite reaching the hundreds on pascals, would not be significant when considering the entire Portuguese population. Given the overpressure values experienced after the 5 km impactor collision, row 3, most locations would experience glass window shattering, severely damaged roofs, and the almost complete collapse of wood-framed buildings. Although the results are certainly worse than the previous two, they fall short of significantly influencing the population.

Table 13. Overpressure vulnerabilities and casualties in Portuguese territory.

		Best		**Expected**		**Worst**	
		C_p	V_p $[10^{-5}]$	C_p	V_p $[10^{-5}]$	C_p	V_p $[10^{-5}]$
1	Mainland	1.4×10^2	1.4	2.2×10^2	2.2	3.2×10^2	3.2
	Azores	1.0	0.4	4.0	1.7	5.0	2.1
	Madeira	3.0	1.2	5.0	2.0	6.0	2.4
2	Mainland	1.3×10^2	1.4	2.2×10^2	2.2	3.1×10^2	3.2
	Azores	1.0	4.1	4.0	1.7	4.0	1.7
	Madeira	3.0	1.2	5.0	2.0	6.0	2.4
3	Mainland	4.0×10^2	4.0	5.0×10^2	5.1	9.7×10^2	9.9
	Azores	5.0	2.1	6.0	2.5	1.5×10^1	6.2
	Madeira	7.0	2.8	1.0×10^1	3.9	2.1×10^1	8.3

The thermal radiation vulnerabilities are divided by case scenario: best, expected, and worst, and into lower and higher thermal radiation. This division means that for every location and case scenario, there are two values for the thermal radiation vulnerabilities and casualties. These thermal radiation thresholds are because of the luminous efficiency, a ratio that defines the amount of kinetic energy converted into thermal radiation. In this study, the luminous efficiency values were set to 10^{-2} for the upper thermal radiation, and 10^{-4} for the lower thermal radiation. In Table 14, the thermal vulnerabilities V_ϕ and casualties C_ϕ can be seen for the upper radiation limit ϕ^+ and the lower limit ϕ^-, for the 5 km impactor case.

Table 14. Thermal vulnerabilities and casualties in Portuguese territory.

		Best		**Expected**		**Worst**	
		C_ϕ	V_ϕ	C_ϕ	V_ϕ	C_ϕ	V_ϕ
ϕ^+	Mainland	2.2×10^6	0.22	4.1×10^6	0.42	8.7×10^6	0.89
	Azores	3.6×10^4	0.15	6.8×10^4	0.28	1.4×10^5	0.60
	Madeira	6.3×10^4	0.25	1.2×10^5	0.47	2.5×10^5	1.0
ϕ^-	Mainland	5.9×10^4	0.006	1.1×10^5	0.011	2.4×10^5	0.024
	Azores	6.6×10^2	0.003	1.2×10^3	0.005	2.6×10^3	0.011
	Madeira	1.1×10^3	0.005	2.2×10^3	0.009	4.6×10^3	0.018

The fireballs generated by Apophis and the medium-asteroid cases would not be wide enough to reach any of the studied locations. The vast distance between the impact site and each municipality would allow the curvature of the Earth to serve as a shield from thermal radiation. As every location would not be directly exposed to radiation, and this model does not emulate radiation reflection or refraction, the vulnerabilities and respective casualties are considered to be zero.

Thermal radiation is the biggest threat from the 5 km impactor collision so far. For mainland Portugal, considering both upper and lower thermal radiation bounds and each case scenario, the vulnerability can range from 0.6% to 89%. The great range of vulnerability values speaks to the uncertainty and the many variables associated with thermal radiation. Despite this, thermal radiation is still a significant threat, as 0.6% of the population represents 5.9×10^4 people. For the Azores Islands, their distance from the impact shields some municipalities from the radiation. However, in the worst-case scenario, the vulnerability reaches 60% of the population, meaning more than 1.4×10^5 people. The tsunami vulnerability can yield values of one in the worst-case scenario, affecting all of its quarter-of-a-million inhabitants.

The ejecta vulnerability is related the ejecta blanket deposit and the likelihood of a building's collapse because of its load. Three different case scenarios were used with the ejecta vulnerability model. The best-case scenario assumes the buildings have a strong frame, the worst-case scenario assumes the buildings are fragile, and the expected case scenario is a compromise between both. The vulnerability after the Apophis impact is irrelevant because the deposition of material deriving from the crater formation is null, and so are the subsequent casualties C_e. There is also no visible difference in each location's vulnerability.

Ejecta is, by definition, material ejected from the impact site during the excavation of the crater. We discussed in Section 3.1 the non-formation of a crater by the medium asteroid at the bottom of the sea. Therefore, its absence means the ejected material is zero, along with the vulnerabilities and casualties. Even though the 5 km impactor generates a significant crater and produces ejected material in the millimetre range that reaches Portugal's mainland and the islands, its consequences are still considered negligible because the upper limit of the fragments' diameter was not assessed.

Portugal is a geographically diverse country. It has coastal regions, exposed to tsunami threats, and mountain ranges, safer from such hazards. The high altitudes of most municipalities are a natural defence from this threat. However, Portugal's vast coast is completely exposed and exhibits vulnerabilities. In Table 15 are displayed the vulnerabilities V_{tsu} and casualties C_{tsu} for the rim waves from the three impacts.

Table 15. Rim-wave vulnerabilities and casualties in Portuguese territory.

		Best		Expected		Worst	
		C_{tsu}	V_{tsu}	C_{tsu}	V_{tsu}	C_{tsu}	V_{tsu}
1	Mainland	7.0×10^5	0.07	1.6×10^6	0.16	2.4×10^6	0.24
	Azores	2.2×10^5	0.90	2.4×10^5	0.99	2.4×10^5	1.0
	Madeira	2.5×10^5	1.0	2.5×10^5	1.0	2.5×10^5	1.0
2	Mainland	1.2×10^5	0.01	3.5×10^5	0.04	8.0×10^5	0.08
	Azores	8.8×10^4	0.36	1.8×10^5	0.74	2.2×10^5	0.89
	Madeira	2.5×10^5	0.99	2.5×10^5	1.0	2.5×10^5	1.0
3	Mainland	7.7×10^6	0.79	7.9×10^6	0.81	7.9×10^6	0.81
	Azores	2.4×10^5	1.0	2.4×10^5	1.0	2.4×10^5	1.0
	Madeira	2.5×10^5	1.0	2.5×10^5	1.0	2.5×10^5	1.0

The Apophis-induced rim wave generates alarming casualty numbers, especially considering that these numbers only represent coastal regions. Considering a Portuguese population of 9.8×10^6 on the mainland, in the best case, 7% of the population is affected by the rim wave, and in the worst-case scenario, the affected population could reach a staggering value of 24%. The situation on the islands is even worse. For the Azores Islands, assuming a population of 2.4×10^4, the rim wave affects 90% to 100% of the population. On Madeira Islands, all the 2.5×10^5 inhabitants are affected, independently of the scenario. For the medium asteroid, the situation is not as dire, except on Madeira Islands because, independent of the scenario, it has casualties over 2.5×10^4. In mainland Portugal, the vulnerability ranges from 1.2% to 8.2%, which is still a significant threat, as those values correspond to 1.2×10^5 and 8.0×10^5 people. On the Azores Islands, the casualties range from over 8.8×10^4 to over 2.2×10^5. For the 5 km impactor, the situation is catastrophic, independently of the scenario. The Azores and Madeira Islands have vulnerabilities of one, and all populations are affected by the first tsunami wave. The vulnerabilities on Portugal's mainland range from 79% to 81%, considering that the tsunami only affects coastal regions.

The vulnerabilities and casualties resulting from the collapse wave would be much lower; see Table 16. For the Apophis asteroid, row 1, in mainland Portugal, the affected population ranges from 0.2% to 2.4%. However, 0.2% of the population is still more than 2.2×10^4, which is still alarming. In the Azores Islands, 7% is the maximum affected population, and in the Madeira Islands, in the worst scenario, 27% of inhabitants would be affected. Regarding the medium asteroid's results, row 2, the vulnerabilities of Portugal's mainland range from 0.2% to 2.2%, and for the Azores Islands, the vulnerabilities range from 0.4% to 4.8%. For Madeira Islands, in the worst-case scenario, the vulnerability reaches 6.7%. Overall, the collapse wave is a lesser threat compared with the rim wave. However, the results on their own are still alarming. As the impact occurred in deep water in these scenarios, the results contradict previous statements [20] that collapse waves are the principal concern in deep oceanic impact events.

Table 16. Collapse wave vulnerabilities and casualties in Portuguese territory.

		Best		Expected		Worst	
		C_{tsu}	V_{tsu}	C_{tsu}	V_{tsu}	C_{tsu}	V_{tsu}
1	Mainland	2.3×10^4	0.002	7.9×10^4	0.008	2.3×10^5	0.024
	Azores	1.4×10^3	0.006	5.7×10^3	0.024	1.8×10^4	0.073
	Madeira	2.8×10^3	0.011	1.9×10^4	0.075	6.8×10^4	0.266
2	Mainland	2.1×10^4	0.002	7.2×10^4	0.007	2.1×10^5	0.022
	Azores	1.1×10^3	0.004	3.9×10^3	0.016	1.2×10^4	0.048
	Madeira	1.3×10^3	0.005	5.3×10^3	0.021	1.7×10^4	0.067

4. Conclusions

The current work studied the short-term effects of three asteroid impacts on Portuguese residents. The celestial objects, assumed to impact the Earth at a 45° angle, included: the Apophis asteroid, a 370-m body, impacting the Earth with a velocity $v_i = 12.62$ km·s^{-1} and a density $\rho_i = 3200$ kg·m^{-3}; a 204-m medium-sized asteroid, representing an NEO threat, assumed to impact the Earth with a velocity $v_i = 10.84$ km·s^{-1} and a density $\rho_i = 3100$ kg·m^{-3}; and an asteroid with a 5-km diameter, impacting the Earth with a velocity $v_i = 15.00$ km·s^{-1} and a density $\rho_i = 2500$ kg·m^{-3}. In addition to the impact assessment for each municipality, the vulnerabilities and the correspondent casualties were assessed for each municipality and each impact effect independently.

Each impact effects assessment included a seismic shaking event, a shock wave, thermal radiation, ejecta deposit, tsunami waves, and the qualitative global effects. The seismic shock could be neglected in the Apophis and medium-asteroid cases, but the 5 km impactor case originated an 8.6 magnitude earthquake. For the 5 km impactor case, the average pressure difference experienced in Portuguese territory because of the shock wave could cause massive structural damage and some potential casualties. However, it was not at all the most concerning threat. The fireball would be big enough to endanger some municipalities, causing thousands of casualties, but again, only for the 5 km impactor case. In all three simulations, the collapse of infrastructure because of the ejecta deposit was the smallest threat. The lack of benthic final crater formation, plus the great distance between the populations and the impact site, should prevent the depositing of ejected material in populated areas. The final impact effect studied was the tsunami. The tsunami would be felt throughout the territory in all three impact events, making it the most concerning impact effect. Regarding global implications, no impact was on a scale big enough to affect the Earth's orbit, rotation period, rotational axis, or mass.

The vulnerability was assessed through pre-established vulnerability models for all the impact effects studied. All the models were subdivided into three case scenarios: best, expected, and worst.

The final estimates were of casualties in every municipality for every impact effect. There was a direct correlation between asteroid impact risk and population density. As such, the casualties were assessed with a simple product relation between the vulnerability and the population.

The rim wave was the most hazardous impact effect for all three impacts, having the highest average vulnerability values. The tsunami wave, independently of the simulation considered, had the ability to destructively affect several hundred-thousand or several million Portuguese people. The thermal radiation for the 5 km impactor could rival the rim wave, as the death toll could reach the millions as well. The impact effects that could be disregarded in terms of threat were the ejecta deposit and the seismic shaking. Even though the 5 km impactor collision estimated a shaking of 8.6 on the Richter scale, the effective magnitude dropped by approximately half, which is enough to be felt, but not enough to cause any real damage to the population.

Author Contributions: Conceptualization, L.F.F.M.S. and R.H.M.; methodology, L.F.F.M.S. and R.H.M.; software, R.H.M.; validation, L.F.F.M.S., A.R.R.S. and R.M.; writing—original draft preparation, R.H.M.; writing—review and editing, L.F.F.M.S., A.R.R.S. and R.M. All authors have read and agreed to the published version of the manuscript.

Funding: This research received no external funding.

Institutional Review Board Statement: Not applicable.

Informed Consent Statement: Not applicable.

Data Availability Statement: Not applicable

Acknowledgments: Fundação para a Ciência e Tecnologia (FCT), under LAETA, through AEROG and IDMEC by project UIDB/50022/2020; by FCT through ICT (Institute of Earth Sciences), project UIDB/04683/2020.

Conflicts of Interest: The authors declare no conflict of interest.

Abbreviations

A_{800}	Wave amplitude at the deep/shallow water threshold
A_{cw}	Collapse wave amplitude
A_{cw}^{max}	Collapse wave maximum amplitude
A_{rw}	Rim-wave amplitude
A_{rw}^{max}	Rim wave maximum amplitude
C_D	Drag coefficient
C_e	Ejecta blanket deposition casualties
C_p	Overpressure casualties
C_{seis}	Seismic shaking casualties
C_{tsu}	Tsunami casualties
C_ϕ	Thermal radiation casualties
D	Distance
D_1	Yield scaled distance
D_c	Threshold diameter between simple and complex craters
d_{fc}	Final crater depth
D_{fc}	Final crater diameter
D_{shore}	Distance between the municipality and the deep/shallow water threshold point
d_{tc}	Transient crater depth
D_{tc}	Transient crater diameter
D_x	Scaled distance
E	Impact energy
E_{kt}	Impact energy in kilotons TNT
f	Ratio of the fireball above the horizon
g_0	Earth standard gravitational acceleration (9.80665 m/s^2)
h_{sea}	Sea depth at impact site
h	Fireball maximum height below the horizon
h_{fr}	Rim height
h_k	Municipality altitude
L	Asteroid diameter
L_e	Mean ejecta fragment diameter
M	Seismic Richter scale magnitude
m_E	Earth mass
m_i	Impactor mass
M_{eff}	Effective seismic Richter scale magnitude
M_i	Impactor linear momentum
R_E	Earth radius
R_f	Fireball radius
p_D	Peak overpressure at distance D
p_e	Load of the ejecta blanket
p_x	Scaled pressure
q	Wave attenuation factor
s	Municipality slope
T_E	Earth rotation period
t_{br}	Breccia lens thickness
t_e	Ejecta blanket thickness
U	Run-up wave height
U_l	Local run-up wave height
V_E	Earth volume
v_E	Earth mean orbital velocity
V_e	Ejecta blanket deposition vulnerability
v_i	Impact velocity

V_p	Overpressure vulnerability
V_{seis}	Seismic shaking vulnerability
V_{tc}	Transient crater volume
V_{tsu}	Tsunami vulnerability
V_ϕ	Thermal radiation vulnerability
Γ_E	Earth angular momentum
Γ_i	Impactor angular momentum
Δ	Epicentral angle
ΔT_E	Change in Earth's length of day
η_{lum}	Luminous efficiency
θ	Asteroid impact angle
λ_i	Impact site longitude
λ_k	Municipality longitude
ρ_i	Impactor density
ρ_t	Target density
ρ_w	Water density
ϕ	Thermal energy per area unit
ϕ_i	Impact site latitude
ϕ_k	Municipality latitude

References

1. Müller, T.G.; Kiss, C.; Scheirich, P.; Pravec, P.; O'Rourke, L.; Vilenius, E.; Altieri, B. Thermal infrared observations of asteroid (99942) Apophis with Herschel. *Astron. Astrophys.* **2014**, *566*, 1–10. [CrossRef]
2. Licandro, J.; Müller, T.; Alvarez, C.; Alí-Lagoa, V.; Delbo, M. GTC/CanariCam observations of (99942) Apophis. *Astron. Astrophys.* **2016**, *585*, 1–4. [CrossRef]
3. Chesley, S.R. Potential impact detection for near-Earth asteroids: The case of 99942 Apophis (2004 MN4). *Proc. Int. Astron. Union* **2005**, *1*, 215–228. [CrossRef]
4. Giorgini, J.D.; Benner, L.A.; Ostro, S.J.; Nolan, M.C.; Busch, M.W. Predicting the Earth encounters of (99942) Apophis. *Icarus* **2008**, *193*, 1–19. [CrossRef]
5. Bancelin, D.; Colas, F.; Thuillot, W.; Hestroffer, D.; Assafin, M. Updated orbit of Apophis with recent observations. In Proceedings of the SF2A 2011: Annual Meeting of the French Society of Astronomy and Astrophysics, Paris, France, 21 June 2011; p. 629.
6. Guo, P.; Ivashkin, V.V.; Stikhno, C.A.; Shkapov, P.M. Determination and investigation of asteroid Apophis' trajectories set potentially colliding with the Earth in 2036. *IOP Conf. Ser. Mater. Sci. Eng.* **2018**, *468*. [CrossRef]
7. Binzel, R.P.; Rivkin, A.S.; Thomas, C.A.; Vernazza, P.; Burbine, T.H.; DeMeo, F.E.; Bus, S.J.; Tokunaga, A.T.; Birlan, M. Spectral properties and composition of potentially hazardous Asteroid (99942) Apophis. *Icarus* **2009**, *200*, 480–485. [CrossRef]
8. Britt, D.T.; Yeomans, D.; Housen, K.; Consolmagno, G. Asteroids Density, Porosity, and Structure. In *Asteroids III*; Bottke, W., Cellino, A., Paolicchi, P., Binzel, R., Eds.; University of Arizona Press: Tucson, AZ, USA, 2002; Volume 4.2, pp. 485–500. [CrossRef]
9. Morais, R.H.; Santos, L.F.F.M.; Silva, A.R.R.; Melicio, R. Hypothetical Apophis deep ocean impact—Energy analysis. *Acta Astronaut.* **2021**, *188*, 438–450. [CrossRef]
10. NASA. NEO Earth Close Approaches. Available online: https://cneos.jpl.nasa.gov/ca/ (accessed on 9 March 2020).
11. Rumpf, C.M.; Lewis, H.G.; Atkinson, P.M. Asteroid impact effects and their immediate hazards for human populations. *Geophys. Res. Lett.* **2017**, *44*, 3433–3440. [CrossRef]
12. Harris, A.W.; Chodas, P.W. The population of near-earth asteroids revisited and updated. *Icarus* **2021**, *365*, 114452. [CrossRef]
13. Rumpf, C.M. Asteroid Impact Risk. Ph.D. Thesis, University of Southampton, Southampton, UK, 2016.
14. Collins, G.S.; Melosh, H.J.; Marcus, R.A. Earth Impact Effects Program: A Web-based computer program for calculating the regional environmental consequences of a meteoroid impact on Earth. *Meteorit. Planet. Sci.* **2005**, *40*, 817–840. [CrossRef]
15. Rumpf, C.M. Global Asteroid Risk Analysis. 2014; pp. 1–10. Available online: http://xxx.lanl.gov/abs/1410.4471 (accessed on 19 February 2019).
16. Rumpf, C.M.; Lewis, H.G.; Atkinson, P.M. *Global Impact Distribution of Asteroids and Affected Population*; 2015. Available online: https://eprints.soton.ac.uk/377825/ (accessed on 19 October 2019).
17. Rumpf, C.; Lewis, H.G.; Atkinson, P.M. Monitoring the Global Asteroid Impact Risk. In Proceedings of the 66th IAF International Astronautical Congress, Jerusalem, Israel, 10 October 2015; Volume IAC-15.B5.
18. Rumpf, C.M.; Lewis, H.G.; Atkinson, P.M. The global impact distribution of Near-Earth objects. *Icarus* **2016**, *265*, 209–217. [CrossRef]
19. Rumpf, C.M.; Lewis, H.G.; Atkinson, P.M. On the influence of impact effect modelling for global asteroid impact risk distribution. *Acta Astronaut.* **2016**, *123*, 165–170. [CrossRef]

20. Wünnemann, K.; Collins, G.S.; Weiss, R. Impact of a cosmic body into Earth's Ocean and the generation of large tsunami waves: Insight from numerical modeling. *Rev. Geophys.* **2010**, *48*, 1–26. [CrossRef]
21. Johnson, B.C.; Collins, G.S.; Minton, D.A.; Bowling, T.J.; Simonson, B.M.; Zuber, M.T. Spherule layers, crater scaling laws, and the population of ancient terrestrial impactors. *Icarus* **2016**, *271*, 350–359. [CrossRef]
22. Collins, G.; Melosh, J. *Errata and Improvements in Earth Impact Effects Program*; 2013. Available online: https://impact.ese.ic.ac.uk/ImpactEarth/ImpactEffects/effects.pdf (acessed on 1 June 2020).
23. Khazins, V.M.; Shuvalov, V.V.; Svettsov, V.V. The Seismic Efficiency of Space Body Impacts. *Sol. Syst. Res.* **2018**, *52*, 547–556. [CrossRef]
24. Matsue, K.; Yasui, M.; Arakawa, M.; Hasegawa, S. Measurements of seismic waves induced by high-velocity impacts: Implications for seismic shaking surrounding impact craters on asteroids. *Icarus* **2020**, *338*, 113520. [CrossRef]
25. Collins, G.S.; Lynch, E.; McAdam, R.; Davison, T.M. A numerical assessment of simple airblast models of impact airbursts. *Meteorit. Planet. Sci.* **2017**, *52*. [CrossRef]
26. Svetsov, V.V.; Shuvalov, V.V. Thermal radiation and luminous efficiency of superbolides. *Earth Planet. Sci. Lett.* **2018**, *503*, 10–16. [CrossRef]
27. Svetsov, V.; Shuvalov, V. Thermal radiation from impact plumes. *Meteorit. Planet. Sci.* **2019**, *54*, 126–141. maps.13200. [CrossRef]
28. Rumpf, C.M.; Lewis, H.G.; Atkinson, P.M. Population vulnerability models for asteroid impact risk assessment. *Meteorit. Planet. Sci.* **2017**, *52*, 1082–1102. [CrossRef]
29. PORDATA. Base de Dados de Portugal Comtemporâneo. Available online: https://www.pordata.pt/Municipios/Altitude+m%c3%a1xima-50 (accessed on 30 April 2020).
30. EMODnet. Undersanding the Topography of the European Seas. Available online: https://portal.emodnet-bathymetry.eu/ (accessed on 4 May 2020).